Colour fields of the quark-antiquark excited flux tube

Pedro Bicudo, Nuno Cardoso and Marco Cardoso

Portuguese Lattice QCD Collaboration

CFTP, Departamento de Física, Instituto Superior Técnico, Universidade de Lisboa, Avenida Rovisco Pais 1, 1049-001 Lisbon, Portugal

Abstract

We present colour field density profiles for some of the first SU(3) gluonic excitations of the flux tube in the presence of a static quark-antiquark pair. The results are obtained from a set of 33 gluonic operators in the space-like Wilson line of the Wilson oop.

1. Introduction

We study the colour fields of the quantum excitations of the pure gauge QCD flux tube produced by a a static quark and a static antiquark. To have enough computer efficiency, we compute the flux tubes with lattice QCD techniques, utilizing NVIDIA GPUS and CUDA codes.

Our goal is to compare the flux tubes with the densities expected in the Nambu-Goto string model. Using the Nambu-Goto string as a model not only helps us to understand the flux tubes, but also to search for deviations from the model, which considers infinitely thin strings, with only transverse quantum excitations.

2. Our 33 operator basis to produce the different excited quantum numbers

In teh study of hybrid excitations [1], we follow the same quantum number notation as in Juge, Kuti and Morningstar [2],

" Three exact quantum numbers which are based on the symmetries of the problem determine the classification scheme of the gluon excitation spectrum in the presence of a static $q\bar{q}$ pair. We adopt the standard notation from the physics of diatomic molecules and use Λ to denote the magnitude of the eigenvalue of the projection $\mathbf{J}_g \cdot \hat{\mathbf{R}}$ of the total angular momentum $\mathbf{J}_g$ of the gluon field onto the molecular axis with unit vector $\hat{\mathbf{R}}$. The capital Greek letters $\Sigma, \Pi, \Delta, \Phi, \ldots$ are used to indicate states with $\Lambda = 0, 1, 2, 3, \ldots$, respectively. The combined operations of charge conjugation and spatial inversion about the midpoint between the quark and the antiquark is also a symmetry and its eigenvalue is denoted by η_{CP}. States with $\eta_{CP} = 1(-1)$ are denoted by the subscripts g (u). There is an additional label for the Σ states; Σ states which are even (odd) under a reflection in a plane containing the molecular axis are denoted by a superscript $+$ $(-)$. Hence, the low-lying levels are labeled Σ_g^+, Σ_g^-, Σ_u^+, Σ_u^-, Π_g, Π_u, Δ_g, Δ_u, and so on. For convenience, we use Γ to denote these labels in general. "

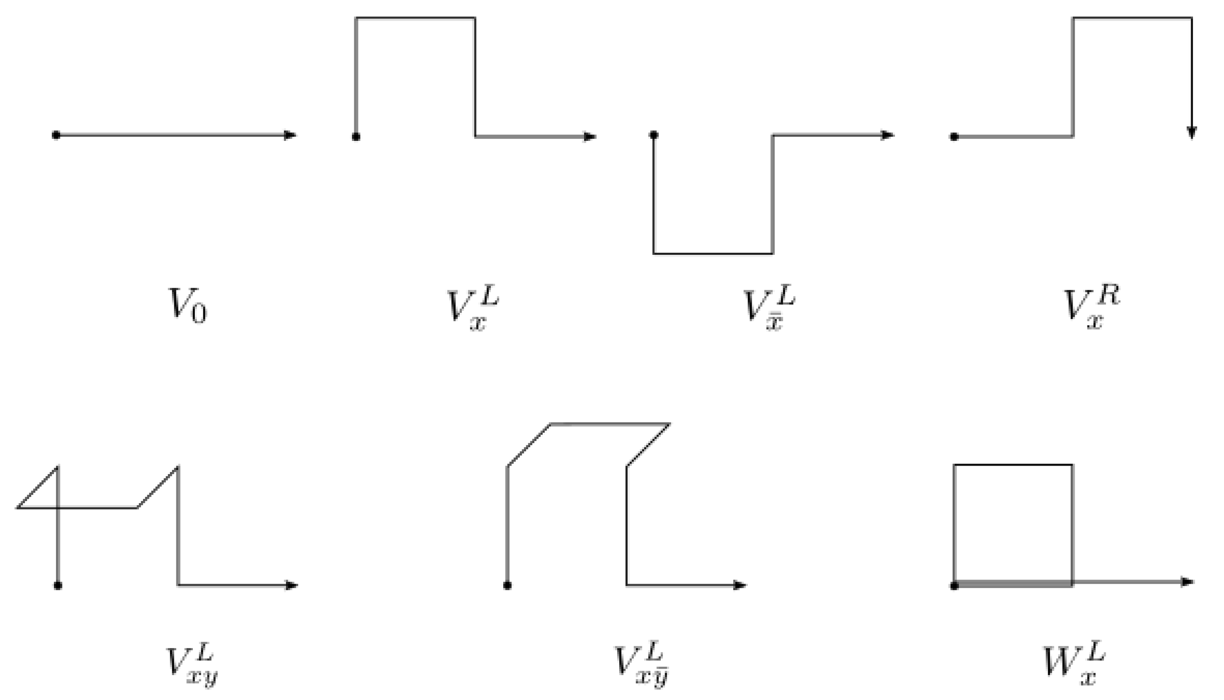

Figure 1: Examples of the paths from the quark to the antiquark used to construct the gauge field operators.labelfig:basisex

We utilize a basis is composed by four kinds of operators:

- The direct operator V_0.
- The eight open-staple operators V_x^L , V_y^L, $V_{\bar{x}}^L$, $V_{\bar{y}}^L$, V_x^R, V_y^R, $V_{\bar{x}}^R$ and $V_{\bar{y}}^R$.
- The sixteen open-staple two-direction operators V_{xy}^L, $V_{x\bar{y}}^L$, $V_{\bar{x}y}^L$, $V_{\bar{x}\bar{y}}^L$, V_{yx}^L, $V_{y\bar{x}}^L$, $V_{\bar{y}x}^L$, $V_{\bar{y}\bar{x}}^L$, V_{xy}^R, $V_{x\bar{y}}^R$, $V_{\bar{x}y}^R$, $V_{\bar{x}\bar{y}}^R$, V_{yx}^R, $V_{y\bar{x}}^R$, $V_{\bar{y}x}^R$ and $V_{\bar{y}\bar{x}}^R$.
- The eight closed-staple operators similar to the open-staple ones W_x^L, etc.

The bar, means that there is displacement in the negative axis direction. The L and R labels indicate whether the staple is on the left or on the right.

This amounts in 33 different operators. With them, we construct operators for the following quantum numbers

- $\boldsymbol{\Sigma_g^+}$

For this quantum number, we have four operators:

$$
\begin{aligned}
\mathcal{A}_{0,1} &= V_0 \\
\mathcal{A}_{0,2} &= \frac{1}{2\sqrt{2}}\left(V_x^L + V_y^L + V_{\bar{x}}^L + V_{\bar{y}}^L + V_x^R + V_y^R + V_{\bar{x}}^R + V_{\bar{y}}^R\right) \\
\mathcal{A}_{0,3} &= \frac{1}{4}\left(V_{xy}^L + V_{x\bar{y}}^L + V_{\bar{x}y}^L + V_{\bar{x}\bar{y}}^L + V_{yx}^L + V_{y\bar{x}}^L + V_{\bar{y}x}^L + V_{\bar{y}\bar{x}}^L\right. \\
&\quad \left. + V_{xy}^R + V_{x\bar{y}}^R + V_{\bar{x}y}^R + V_{\bar{x}\bar{y}}^R + V_{yx}^R + V_{y\bar{x}}^R + V_{\bar{y}x}^R + V_{\bar{y}\bar{x}}^R\right) \\
\mathcal{A}_{0,4} &= \frac{1}{2\sqrt{2}}\left(W_x^L + W_y^L + W_{\bar{x}}^L + W_{\bar{y}}^L + W_x^R + W_y^R + W_{\bar{x}}^R + W_{\bar{y}}^R\right)
\end{aligned}
$$

- $\boldsymbol{\Sigma_u^+}$

For this quantum number, we have three operators:

$$
\begin{aligned}
\mathcal{A}_{2,1} &= \frac{1}{2\sqrt{2}}\left(V_x^L + V_y^L + V_{\bar{x}}^L + V_{\bar{y}}^L - (V_x^R + V_y^R + V_{\bar{x}}^R + V_{\bar{y}}^R)\right) \\
\mathcal{A}_{2,2} &= \frac{1}{4}\left(V_{xy}^L + V_{x\bar{y}}^L + V_{\bar{x}y}^L + V_{\bar{x}\bar{y}}^L + V_{yx}^L + V_{y\bar{x}}^L + V_{\bar{y}x}^L + V_{\bar{y}\bar{x}}^L\right. \\
&\quad \left. -(V_{xy}^R + V_{x\bar{y}}^R + V_{\bar{x}y}^R + V_{\bar{x}\bar{y}}^R + V_{yx}^R + V_{y\bar{x}}^R + V_{\bar{y}x}^R + V_{\bar{y}\bar{x}}^R)\right) \\
\mathcal{A}_{2,3} &= \frac{1}{2\sqrt{2}}\left(W_x^L + W_y^L + W_{\bar{x}}^L + W_{\bar{y}}^L - (W_x^R + W_y^R + W_{\bar{x}}^R + W_{\bar{y}}^R)\right)
\end{aligned}
$$

- $\boldsymbol{\Pi_u}$

Four operators for these quantum numbers:

$$
\begin{aligned}
\mathcal{A}_{4,1} &= \frac{1}{2\sqrt{2}}\left(V_x^L + iV_y^L - V_{\bar{x}}^L - iV_{\bar{y}}^L + V_x^R + iV_y^R - V_{\bar{x}}^R - iV_{\bar{y}}^R\right) \\
\mathcal{A}_{4,2} &= \frac{1}{4}\left(V_{xy}^L + V_{x\bar{y}}^L - V_{\bar{x}y}^L - V_{\bar{x}\bar{y}}^L + iV_{yx}^L + iV_{y\bar{x}}^L - iV_{\bar{y}x}^L - iV_{\bar{y}\bar{x}}^L + V_{xy}^R + V_{x\bar{y}}^R - V_{\bar{x}y}^R - V_{\bar{x}\bar{y}}^R + iV_{yx}^R + iV_{y\bar{x}}^R - iV_{\bar{y}x}^R - iV_{\bar{y}\bar{x}}^R\right) \\
\mathcal{A}_{4,3} &= \frac{1}{4}\left(V_{xy}^L - V_{x\bar{y}}^L + V_{\bar{x}y}^L - V_{\bar{x}\bar{y}}^L - iV_{yx}^L + iV_{y\bar{x}}^L - iV_{\bar{y}x}^L + iV_{\bar{y}\bar{x}}^L + V_{xy}^R - V_{x\bar{y}}^R + V_{\bar{x}y}^R - V_{\bar{x}\bar{y}}^R - iV_{yx}^R + iV_{y\bar{x}}^R - iV_{\bar{y}x}^R + iV_{\bar{y}\bar{x}}^R\right) \\
\mathcal{A}_{4,4} &= \frac{1}{2\sqrt{2}}\left(W_x^L + iW_y^L - W_{\bar{x}}^L - iW_{\bar{y}}^L + W_x^R + iW_y^R - W_{\bar{x}}^R - iW_{\bar{y}}^R\right)
\end{aligned}
$$

3. Computation of the chromofields in the flux tube

The central observables that govern the event in the flux tube can be extracted from the correlation of a plaquette, $\square_{\mu\nu}$, with the Polyakov loops, L,

$$f_{\mu\nu}(R,x) = \frac{\beta}{a^4}\left[\frac{\langle \mathcal{W}\,\square_{\mu\nu}(x)\rangle}{\langle \mathcal{W}\rangle} - \langle \square_{\mu\nu}(x)\rangle\right] \tag{1}$$

where W is the quark-antiquark Wilson loop, x denotes the distance of the plaquette from the line connecting quark sources, R is the quark separation.

Therefore, using the plaquette orientation $(\mu,\nu) = (2,3), (1,3), (1,2), (1,4), (2,4), (3,4)$, we can relate the six components in Eq. (1) to the components of the chromoelectric and chromomagnetic fields,

$$f_{\mu\nu} \to \left(-\langle B_x^2\rangle, -\langle B_y^2\rangle, -\langle B_z^2\rangle, \langle E_x^2\rangle, \langle E_y^2\rangle, \langle E_z^2\rangle\right) \tag{2}$$

and also calculate the total action (Lagrangian) density, $\langle \mathcal{L}\rangle = \frac{1}{2}\left(\langle E^2\rangle - \langle B^2\rangle\right)$.

In order to improve the signal over noise ratio, we use multihit technique in the temporal Wilson lines and the APE smearing spatial Wilson lines.

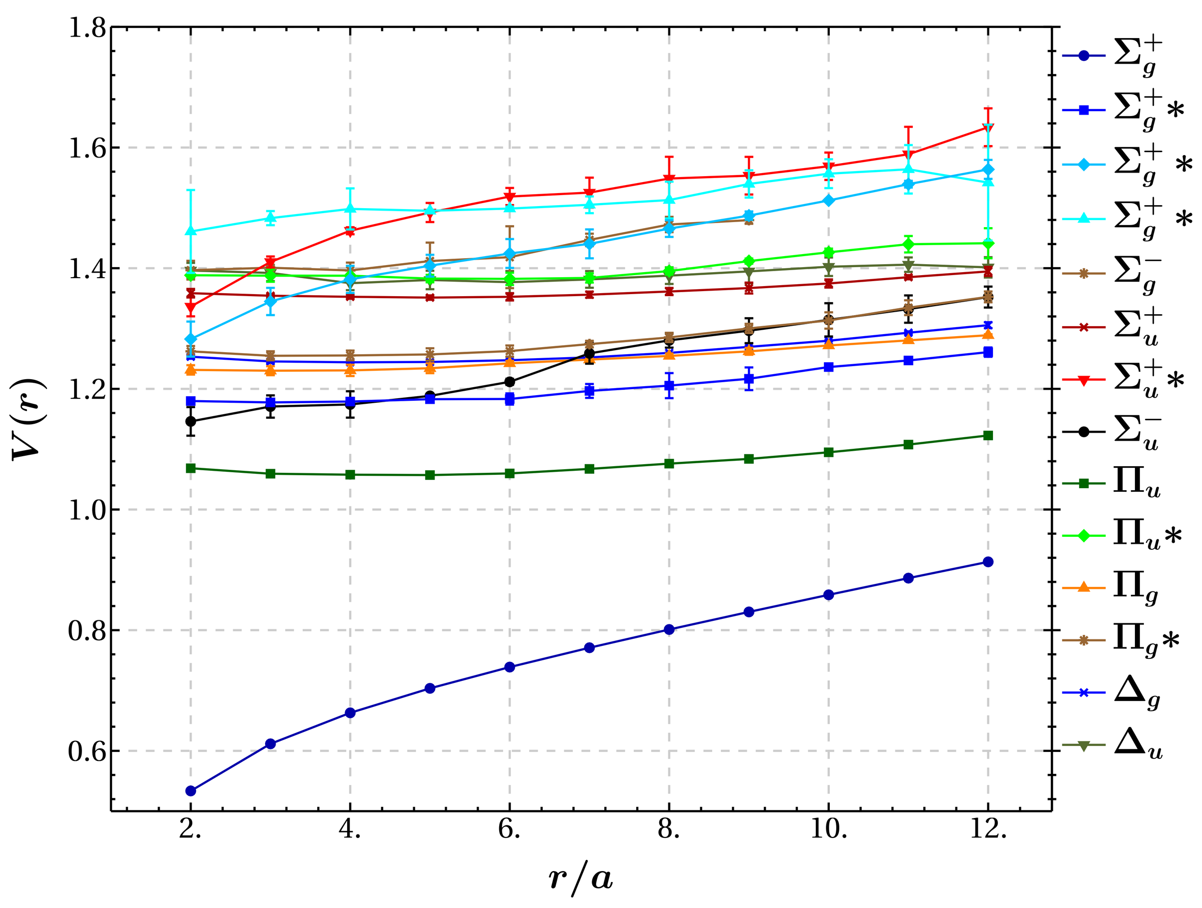

Figure 2: V(r)

4. Configuration ensemble and code efficiency

In this section, we present the results using 1199 configurations for a fixed lattice volume of $24^3 \times 48$ and $\beta = 6.2$. We present our results in lattice spacing units of a, with $a = 0.07261(85)$ fm or $a^{-1} = 2718(32)$ MeV. The the quark and antiquark are located at $(0,0,-R/2)$ and $(0,0,R/2)$ for R between 6 and 10 in lattice spacing units.

All our computations are performed in NVIDIA GPUs using our CUDA codes. The computation of the chromofields are very compute intensive and due to GPU limited memory this requires an intensive use of atomic memory operations. For example, to calculate the fields for the Σ_u^+ in the GeForce GTX TITAN Black, it takes approximately 83 minutes.

5. Results

Our results are presented in figures 2 to 5. The ground-state Σ_g^+ is the familiar static-quark potential [3], figure 2. The lowest-lying excitation is the Π_u.

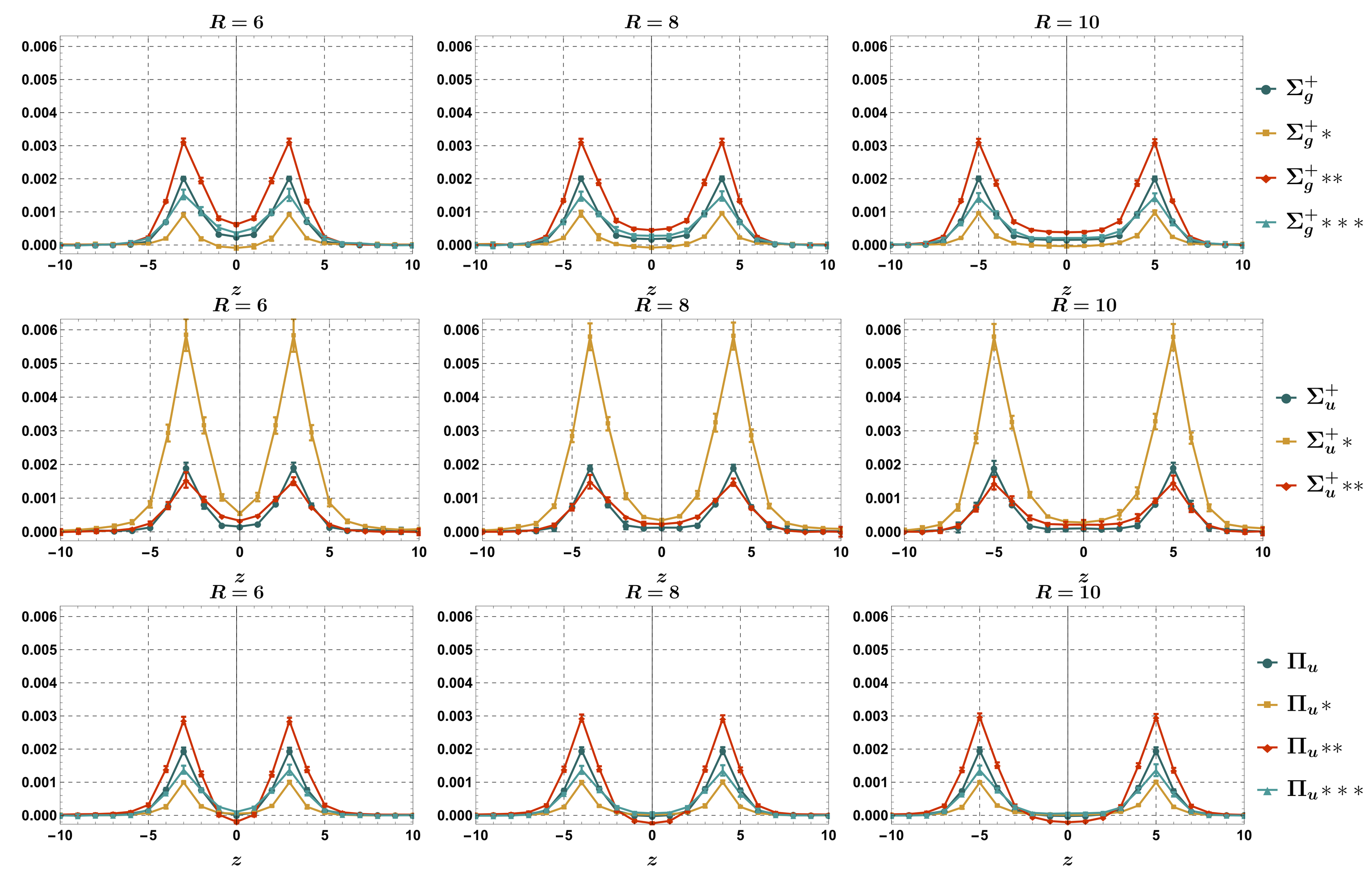

Figure 3: Lagrangian density in the charges axis

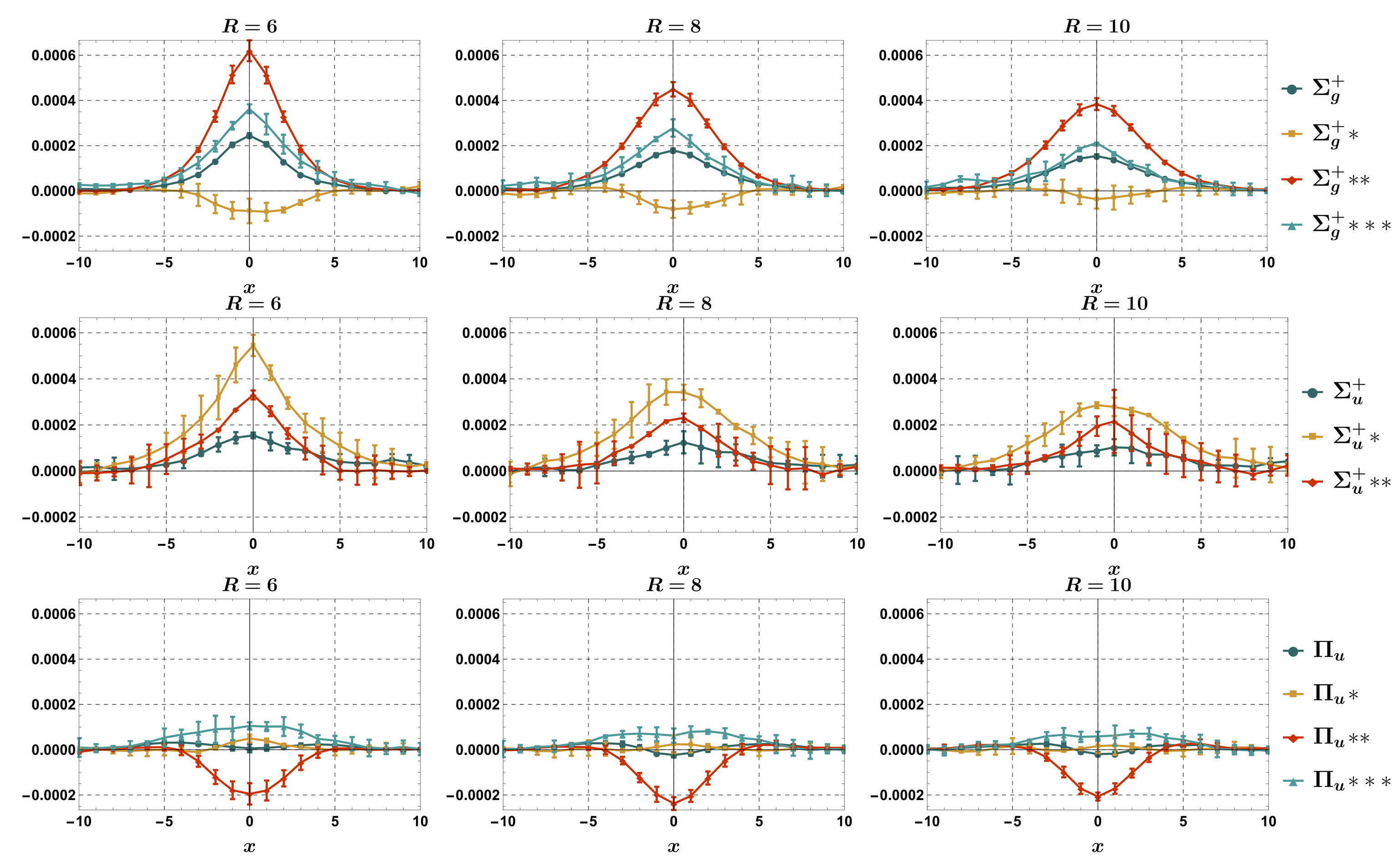

Figure 4: Lagrangian density in the mediator plane

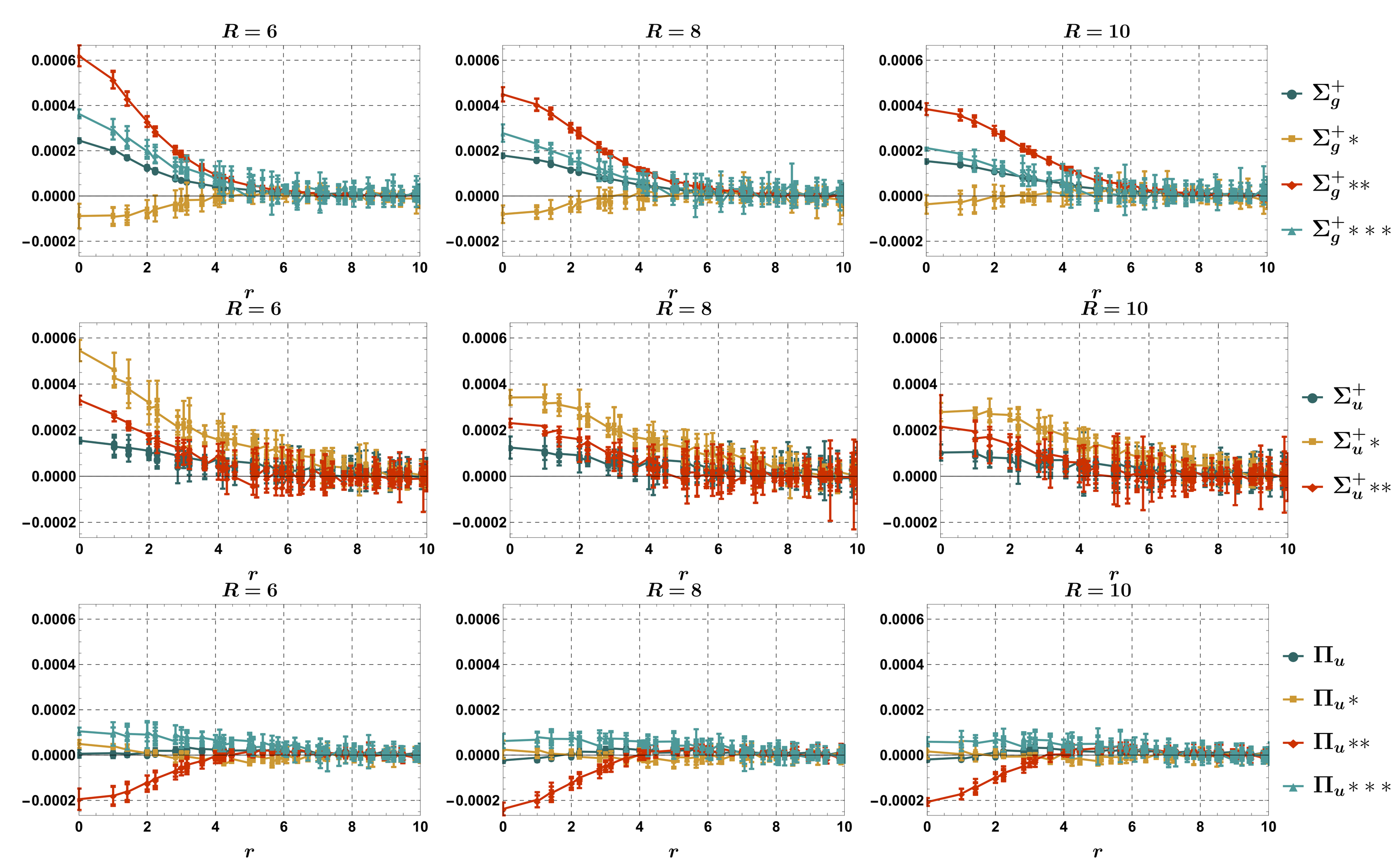

Figure 5: Lagrangian density in the mediator plane

6. Conclusions

We compute the potentials for several excitations of the flux tube, but for the colour field square densities we only select the main excited states in each quantum number.

We consider radial excitations of the groundstate Σ_g^+, the first angular excitation Π_u and the first axial parity excitation Σ_u^+.

In our results, we show the Lagrangian density in the charge axis in in Fig. 3: We also compare the Lagrangian density in the mediator plane in one axis only in Fig. 4 with the average in different mediator plane axis in Fig. 5.

As a preliminary result, we find states consisten with the transverse excitations of the Nambu-Goto string model, but we also find states who may correspond to excitations beyond the model.

Acknowledgements

Nuno Cardoso and Marco Cardoso are supported by FCT under the contracts SFRH/BPD/109443/2015 and SFRH/BPD/73140/2010 respectively. We also acknowledge the use of CPU and GPU servers of PtQCD, supported by NVIDIA, CFTP and FCT grant UID/-FIS/00777/2013.

References

- P. Lacock, C. Michael, P. Boyle, P. Rowland, Orbitally excited and hybrid mesons from the lattice, Phys. Rev. D54 (1996) 6997–7009.
  arXiv:hep-lat/9605025, doi:10.1103/PhysRevD.54.6997.
- K. J. Juge, J. Kuti, C. Morningstar, Fine structure of the QCD string spectrum, Phys. Rev. Lett. 90 (2003) 161601.
  arXiv:hep-lat/0207004, doi:10.1103/PhysRevLett.90.161601.
- N. Cardoso, M. Cardoso, P. Bicudo, Inside the SU(3) quark-antiquark QCD flux tube: screening versus quantum widening, Phys. Rev. D88 (2013) 054504.
  arXiv:1302.3633, doi:10.1103/PhysRevD.88.054504.